ChemComm

COMMUNICATION

View Article Online
View Journal | View Issue

Cite this: *Chem. Commun.*, 2024, **60**, 11112

Received 25th July 2024,
Accepted 7th September 2024

DOI: 10.1039/d4cc03757j

rsc.li/chemcomm

Engineering heterostructured Mo_2C/MoS_2 catalyst with hydrophilicity/aerophobicity *via* carbothermal shock for efficient alkaline hydrogen evolution†

Hao Xiong, Xinren Zhang, Xu Peng, Dengke Liu, Yimeng Han and Fei Xu *

The exploration of high-performance hydrogen evolution reaction (HER) catalysts is conducive to the development of clean hydrogen energy, yet still remains a challenge. Herein, we rapidly synthesize the Mo_2C/MoS_2 heterostructure on carbon paper (Mo_2C/MoS_2–CP) *via* carbothermal shock in only two seconds. The construction of the Mo_2C/MoS_2 heterostructure regulates the electronic structure of the Mo site and facilitates charge transfer during the HER process. Moreover, the catalyst exhibits enhanced hydrophilicity and aerophobicity, facilitating optimal electrolyte–catalyst interaction and efficient hydrogen bubble detachment for accelerated mass transfer. Consequently, Mo_2C/MoS_2–CP exhibits superior intrinsic alkaline HER activity, and excellent stability for 100 h. This finding provides a novel insight into the development of outstanding HER catalysts.

Excessive consumption of fossil fuels has caused serious environmental pollution and energy depletion, giving rise to an urgent need for the development of renewable and clean energy.[1,2] Due to the high specific energy density and zero carbon emission, hydrogen from alkaline water electrolysis is regarded as one of the promising alternative energy resources, which has been developed for hundreds of years.[3] As an essential half-reaction in electrochemical water splitting, the hydrogen evolution reaction (HER) is not spontaneous and involves intricate solid–liquid–gas triple-phase interfaces, which requires well-designed catalysts to reduce the HER overpotential and facilitate the interfacial mass transfer.[4] Currently, Pt-based catalysts are considered to be the best alkaline HER catalysts owing to their high activity with low overpotential and rapid reaction kinetics, but severely restricted by their scarcity, high cost, and limited durability.[5] Therefore, it is imperative to develop alkaline HER catalysts with low-cost and high activity to substitute for Pt-based catalysts.

State Key Laboratory of Solidification Processing, Center for Nano Energy Materials, School of Materials Science and Engineering, Northwestern Polytechnical University, Xi'an 710072, P. R. China. E-mail: feixu@nwpu.edu.cn

† Electronic supplementary information (ESI) available. See DOI: https://doi.org/10.1039/d4cc03757j

Among various non-precious metal catalysts, molybdenum disulfide (MoS_2) is a typical transition metal dichalcogenide and a promising alternative to Pt-based catalysts owing to the low-cost and potential marginal active sites.[6,7] However, the poor conductivity and inert coordination-saturated atoms in the basal plane pose a great challenge to the overall catalytic activity.[4,8] To this end, various strategies such as heteroatom doping,[9,10] defect engineering,[11–13] and phase or structure engineering,[14–17] have been developed to activate catalytic sites and regulate the electronic structure, enhancing the intrinsic HER activity of MoS_2. In particular, the implementation of phase or structure engineering has been extensively demonstrated as an effective strategy for mitigating the HER overpotential of MoS_2-based catalysts. For instance, 1T-2H MoS_2,[18] Co–BDC/MoS_2,[19] and NiS_2/MoS_2,[20] were designed with decreased overpotential down to 204 mV at the low current density of 10 mA cm^{-2}. Despite these advances, concerns still exist on achieving remarkably lower overpotential (*e.g.* <200 mV).[21–23] The primary reason is that the aforementioned MoS_2-based catalysts only focus on realizing fast charge transfer through structural modulation, and lack proper modifications of surface properties such as hydrophilicity and aerophobicity, which involves achieving rapid diffusion of the electrolyte, accessibility of the active sites, and timely detachment of hydrogen bubbles.[4,24] In particular at large current densities (>100 mA cm^{-2}), numerous hydrogen bubbles will be generated to cover the surface of the catalysts, which prevents the active sites from contacting the electrolyte and results in a dramatic fluctuation and deterioration of the HER performance.[25,26] Therefore, apart from facilitating charge transfer, modulating surface properties for accelerated mass transfer at the solid–liquid–gas interfaces is also essential but still challenging.[27,28] In this sense, it is of scientific significance to engineer MoS_2-based catalysts with exceptional activity *via* structure engineering, enabling simultaneous achievement of rapid charge and mass transfer.

In this context, we prepared a self-supported catalyst consisting of a Mo_2C/MoS_2 heterostructure constructed on carbon paper (Mo_2C/MoS_2–CP) through ultrafast carbothermal shock within 2 seconds. The consciously constructed Mo_2C/MoS_2 heterostructure effectively modulates the electronic structure

of the active Mo sites. Meanwhile, the catalyst displays excellent hydrophilicity and aerophobicity, which facilitates rapid wetting of the active sites by the electrolyte and the timely release of hydrogen bubbles, especially at large current densities. Consequently, we simultaneously realized the fast transfer of both charge and mass during the HER process. As a result, Mo_2C/MoS_2–CP exhibits a significantly reduced overpotential and low Tafel slope of 64.5 mV dec^{-1}, demonstrating superior HER kinetics. Besides, Mo_2C/MoS_2–CP can also work stably for 100 h, suggesting excellent alkaline HER stability. This finding successfully achieves the synergistic promotion of HER kinetics by the structure and surface properties of MoS_2-based catalysts through the structure engineering strategy.

Compared to the conventional tube furnace with a heating cycle of several hours and the gas heat transfer, this ultrafast carbothermal shock has a short heating cycle of only a few seconds, thereby maximizing the utilization of generated heat for efficient temperature elevation of materials. Meanwhile, it is expected to overcome the oxidation, aggregation, and deactivation of active centres appearing in the conventional heating process, and thus abundant active centres can be obtained for the HER process.[29,30] In this regard, we prepared Mo_2C/MoS_2–CP catalysts by a facile solution impregnation and ultrafast carbothermal shock method (Fig. 1a). Mo_2C was formed with the Mo source ammonium molybdate tetrahydrate and the C source glucose during the carbothermal shock process. The heating and cooling process is instantaneously accomplished within 2 seconds with temperatures up to 1500 °C (Fig. S1a, ESI†). Stacked MoS_2 nanosheets firmly attached to carbon fibres in the Mo_2C/MoS_2–CP catalysts with uniform distribution of C, S, and Mo (Fig. 1b, c and f). The high-resolution TEM (HRTEM) image reveals that there are two types of crystalline regions with different orientations and their heterointerface forming at the edges of the MoS_2 nanosheets in Fig. 1d. Among them, the lattice spacings of 0.25 nm and 0.235 nm belong to the (102) plane of MoS_2 and the (200) plane of Mo_2C, respectively (Fig. 1d and e). Meanwhile, control samples of CP, Mo_2C-CP, and MoS_2–CP were also prepared (Fig. S2–S5, ESI†). There is only a single phase present in MoS_2 flakes or Mo_2C nanoparticles (Fig. S4 and S5, ESI†).

To better understand the structure of the Mo_2C/MoS_2–CP catalyst, the X-ray diffraction patterns (XRD) and X-ray photoelectron spectroscopy (XPS) spectra have been conducted as shown in Fig. 2. Due to the existence of the highly graphitized carbon fibre substrate, the sharp diffraction peaks of the (002) plane and (004) plane of graphite (PDF#89-8487) appear in all samples of the Mo_2C-CP, MoS_2–CP, and Mo_2C/MoS_2–CP (Fig. 2a and Fig. S6a, ESI†). The diffraction patterns ascribed to MoS_2 (PDF#77-1716) and Mo_2C (PDF#77-0720) are both present in the Mo_2C/MoS_2–CP (Fig. 2a). Consequently, the Mo_2C/MoS_2 heterostructure has been successfully constructed on the CP substrate *via* carbothermal shock. Furthermore, the survey spectra in Fig. 2b manifest the existence of C, Mo, and S elements in Mo_2C/MoS_2–CP and MoS_2–CP, while no Mo in CP and S in the Mo_2C-CP, different from that found in MoS_2-CP (Fig. S6b–d, ESI†). As for the C 1s spectra, additional Mo–C peaks are also observed in Mo_2C/MoS_2–CP and Mo_2C-CP, apart from the C–C and C–O two peaks located at 284.8 eV and 285.7 eV in all samples (Fig. 2c). However, there exists a 0.2 eV negative shift in Mo_2C/MoS_2–CP probably due to the formation of the heterostructure (Fig. 2c). Most studies have indicated that Mo is dominated by Mo^{2+} in Mo_2C and Mo^{4+} in MoS_2.[28,31] As shown in Fig. 2d, the multiple valence states of Mo suggest the presence of both Mo_2C and MoS_2 phases in the Mo_2C/MoS_2–CP. Moreover, the Mo^{2+} peaks in Mo_2C/MoS_2–CP are negatively shifted by ~0.2 eV, and the Mo^{2+} content of Mo_2C/MoS_2–CP (~33.9%) is higher than that of Mo_2C-CP (~24%), which indicated that the valence state and electronic structure of Mo have been regulated by the Mo_2C/MoS_2 heterostructure, promoting charge transfer and activating the potential reaction sites.[32,33]

The HER process occurs at the electrode–electrolyte interface, and the transfer of masses such as the electrolyte and the

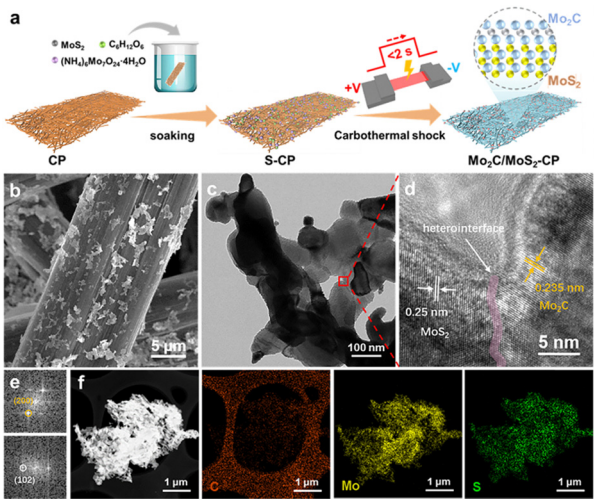

Fig. 1 (a) Schematic illustration of the synthesis of Mo_2C/MoS_2–CP by ultra-fast heating; (b) SEM, (c) TEM and (d) HRTEM images of Mo_2C/MoS_2–CP; (e) fast Fourier transform patterns of Mo_2C (up) and MoS_2 (down) from figure (d); (f) the HAADF-STEM image and corresponding elemental mappings of Mo_2C/MoS_2–CP.

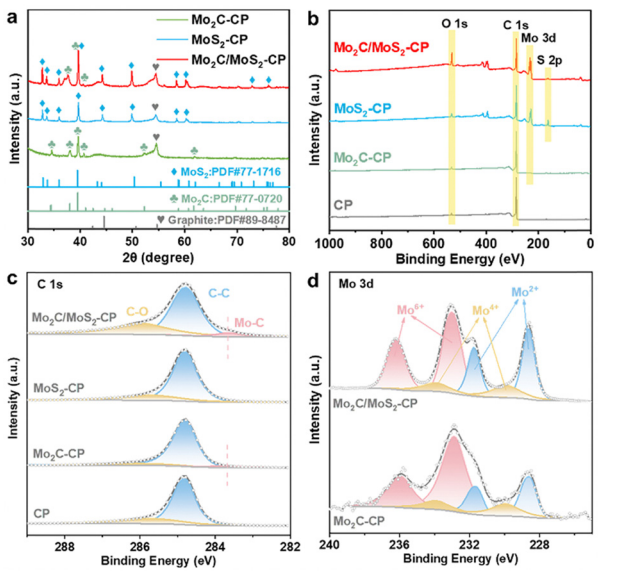

Fig. 2 (a) XRD patterns of Mo_2C-CP, MoS_2–CP, and Mo_2C/MoS_2–CP; (b) XPS survey spectra; XPS spectra of (c) C 1s and (d) Mo 3d.

timely generation of hydrogen bubbles at this solid–liquid interface significantly affect the HER rate, especially under large current densities. Hence, it is desirable to conduct a comprehensive investigation into the behaviors of the electrolyte and hydrogen bubbles at the catalyst surface. As shown in the dynamic contact angle test in Fig. 3a, the contact angle of the KOH electrolyte droplet on the Mo_2C/MoS_2–CP surface is 47.6° at an interval of 2 s, which is much smaller than that observed on the CP surface (138.5°). We further find that the Mo_2C/MoS_2–CP surface is completely wetted by the electrolyte with a contact angle of 0° after 3 s, while the CP surface maintains a large wetting angle even after 20 s. Therefore, the Mo_2C/MoS_2–CP surface exhibits enhanced wettability than CP. The superior hydrophilicity facilitates rapid replenishment of the electrolyte consumed during the HER, thereby boosting the fast alkaline HER kinetics, especially at high current densities. Consequently, the detachment behaviors of hydrogen bubbles on the surfaces of CP and Mo_2C/MoS_2–CP electrodes differ radically. Obviously, the CP surface is densely covered with a multitude of large-sized hydrogen bubbles, while only a limited number of smaller hydrogen bubbles are adsorbed onto the Mo_2C/MoS_2–CP surface under high current densities (Fig. 3b). In the case of that at 100 mA cm^{-2}, approximately 81.2% of the hydrogen bubbles on the CP surface exhibit size growth ranging from 0.2–0.3 mm or even up to 0.7–0.8 mm, while predominantly small-sized hydrogen bubbles in the range of 0.1–0.2 mm on the Mo_2C/MoS_2–CP (Fig. 3c), indicative of the aerophobic property of Mo_2C/MoS_2–CP surface. Specifically, the presence of large-sized bubbles covers many active sites, hampering the interaction between the active sites and electrolyte and hindering the new HER process.[26] As a result, the heterostructure engineering improves the hydrophilicity and aerophobicity, indicative of the rapid-released hydrogen bubbles and quick-wetted re-exposure of the active sites, thus accelerating the alkaline HER kinetics.

The HER performance of the as-prepared electrocatalysts was evaluated in 1 M KOH electrolyte. By systematically optimizing the holding times and precursor ratios, we found that the Mo_2C/MoS_2–CP without holding time and with molar ratio ($(NH_4)_6Mo_7O_{24}{\cdot}4H_2O$: MoS_2) of 3 : 1 exhibited optimal alkaline HER performance of the lowest overpotential (Fig. S1, S7 and Table S1, ESI†). As depicted in Fig. 4a, Mo_2C/MoS_2–CP showcases superior alkaline HER performance than Mo_2C-CP and MoS_2–CP. Mo_2C/MoS_2–CP shows smooth manifestation *via* the linear sweep voltammetry (LSV) curves, in sharp contrast to the presence of significant polarization using Mo_2C-CP, MoS_2–CP, and Pt/C at large current densities. To reach the current densities of 10, 100, and 300 mA cm^{-2}, Mo_2C/MoS_2–CP only needs the overpotentials of 191.4 mV, 258.4 mV, and 310.8 mV, respectively, which are lower than those of Mo_2C-CP (257.5 mV, 408.3 mV, and 579.4 mV) and MoS_2–CP (214.4 mV, 365.9 mV, and 568.1 mV) and slightly higher than Pt/C (Fig. S8a and Table S2, ESI†). Meanwhile, Mo_2C/MoS_2–CP also shows a Tafel slope of 64.5 mV dec^{-1}, which is lower than that of Mo_2C-CP (113.1 mV dec^{-1}) and MoS_2–CP

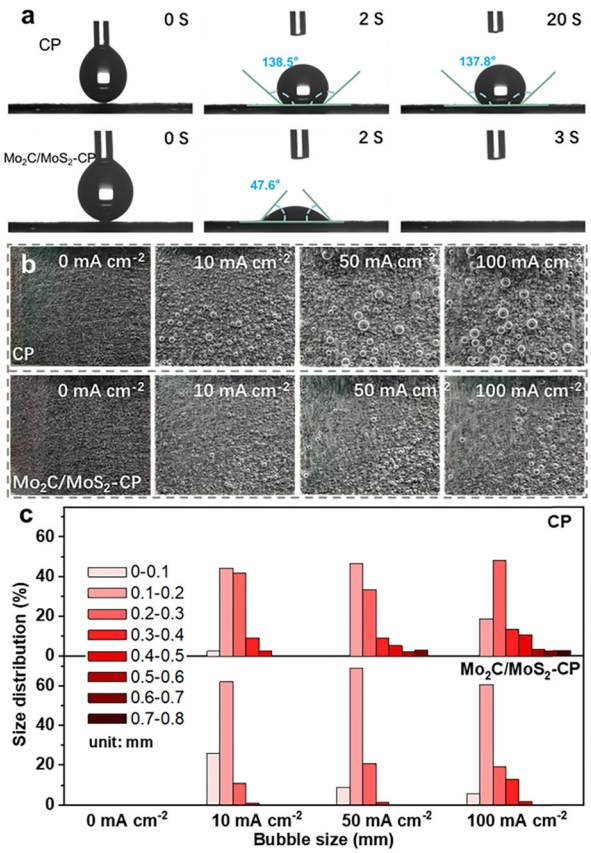

Fig. 3 (a) Contact angles of CP (up) and Mo_2C/MoS_2–CP (down); (b) digital images and (c) corresponding hydrogen bubble size distributions for the HER at 0, 10, 50, and 100 mA cm^{-2} of CP and Mo_2C/MoS_2–CP.

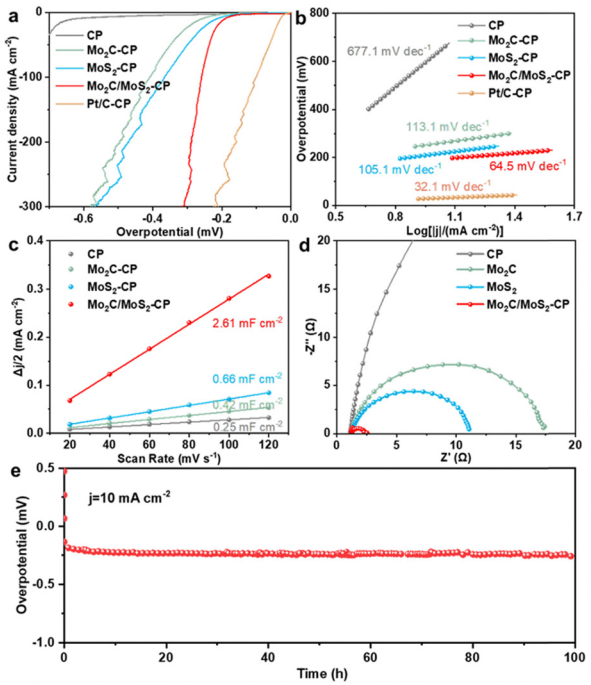

Fig. 4 (a) LSV curves in 1 M KOH, (b) Tafel curves, (c) C_{dl} values, and (d) Nyquist plots of CP, Mo_2C-CP, MoS_2–CP, and Mo_2C/MoS_2–CP, and the Pt/C-CP was also provided in (a) and (b); (e) chronoamperometry curve of Mo_2C/MoS_2–CP at 10 mA cm^{-2} in 1 M KOH.

(105.1 mV dec^{-1}) but slightly larger than Pt/C (32.1 mV dec^{-1}), demonstrating the fast alkaline HER kinetics (Fig. 4b). Clearly, Mo_2C/MoS_2–CP still has both exceptional overpotential and Tafel slope compared to the reported phase or structure-engineered MoS_2-based catalysts, suggesting that the simultaneous improvement of charge and mass transfer by a structure engineering strategy for enhancing the catalytic performance holds great promise (Table S3, ESI†).

The intrinsic catalytic activity of the catalysts was further evaluated by normalizing in terms of the electrochemical active surface area (ECSA) estimated from electrochemical double-layer capacitance (C_{dl}). Mo_2C/MoS_2–CP exhibits the largest C_{dl} of 2.61 mF cm^{-2}, greatly larger than that of MoS_2–CP (0.66 mF cm^{-2}), Mo_2C-CP (0.42 mF cm^{-2}), and CP (0.25 mF cm^{-2}), respectively (Fig. 4c and Fig. S9, ESI†). Correspondingly, the largest ECSA suggests more active sites in the Mo_2C/MoS_2–CP catalyst available for the HER (Table S4, ESI†). Furthermore, the LSV curves with the current density normalized by ECSA (j_{ECSA}) indicate the lower overpotential of Mo_2C/MoS_2–CP than that of Mo_2C-CP and MoS_2–CP when j_{ECSA} exceeds 3.0 mA cm^{-2} and 10.0 mA cm^{-2}, respectively, demonstrating excellent intrinsic HER activity (Fig. S8b, ESI†). Therefore, the construction of the Mo_2C/MoS_2 heterostructure activates more active sites, by increasing the density of active sites and enhancing the catalytic activity. As shown in the Nyquist plots (Fig. 4d), Mo_2C/MoS_2–CP exhibits the smallest charge transfer resistance (R_{ct}) of 1.2 Ω compared to Mo_2C-CP (16.1 Ω), MoS_2–CP (10.0 Ω), and CP (132.2 Ω), further indicating the rapid charge transfer during the HER (Table S5, ESI†). Additionally, with continuous HER at 10 mA cm^{-2}, the Mo_2C/MoS_2–CP catalyst remains stable for 100 h after only a small increase in overpotential at the start of electrolysis (Fig. 4e). Meanwhile, the SEM image after the chronoamperometry test confirms the stable structure of Mo_2C/MoS_2–CP (Fig. S10, ESI†).

In summary, the hydrophilic and aerophobic Mo_2C/MoS_2–CP catalyst was rapidly synthesized *via* carbothermal shock. The successful construction of the Mo_2C/MoS_2 heterostructure with hydrophilic/aerophobic surface design achieved favorable charge and mass transfer, effectively enhancing the alkaline HER performance of the catalysts. This finding provides new insights into the design of high-performance alkaline HER catalysts through the structure engineering strategy and ultrafast heating technique.

This work was financially supported by the project of the National Natural Science Foundation of China (52322203, 52473220) and the Key Research and Development Program of Shaanxi Province (2024GH-ZDXM-21).

Data availability

The data supporting this article have been included as part of the ESI.†

Conflicts of interest

There are no conflicts to declare.

Notes and references

1 Z. W. Seh, J. Kibsgaard, C. F. Dickens, I. Chorkendorff, J. K. Norskov and T. F. Jaramillo, *Science*, 2017, **355**, 146.
2 P. Zhou, I. A. Navid, Y. Ma, Y. Xiao, P. Wang, Z. Ye, B. Zhou, K. Sun and Z. Mi, *Nature*, 2023, **613**, 66–70.
3 Z. Y. Yu, Y. Duan, X. Y. Feng, X. X. Yu, M. R. Gao and S. H. Yu, *Adv. Mater.*, 2021, **33**, 2007100.
4 W. Han, J. Ning, Y. Long, J. Qiu, W. Jiang, Y. Wang, L. A. Shah, D. Yang, A. Dong and T. Li, *Adv. Energy Mater.*, 2023, **13**, 2300145.
5 H. G. Han, J. W. Choi, M. Son and K. C. Kim, *eScience*, 2024, **4**, 100204.
6 Z. Yin, X. Liu, S. Chen, T. Ma and Y. Li, *Energy Environ. Mater.*, 2022, **6**, e12310.
7 C. Zhang, Y. Luo, J. Tan, Q. Yu, F. Yang, Z. Zhang, L. Yang, H.-M. Cheng and B. Liu, *Nat. Commun.*, 2020, **11**, 3724.
8 X. Liu, X. Jiang, G. Shao, H. Xiang, Z. Li, Y. Jin, Y. Chen, H. Jiang, H. Li, J. Shui, Y. Feng and S. Liu, *Small*, 2022, **18**, 2200601.
9 Y. Qian, J. Yu, Z. Lyu, Q. Zhang, T. H. Lee, H. Pang and D. J. Kang, *Carbon Energy*, 2023, **6**, e376.
10 J. Hu, B. L. Huang, C. X. Zhang, Z. L. Wang, Y. M. An, D. Zhou, H. Lin, M. K. H. Leung and S. H. Yang, *Energy Environ. Sci.*, 2017, **10**, 593–603.
11 J. Xu, G. Shao, X. Tang, F. Lv, H. Xiang, C. Jing, S. Liu, S. Dai, Y. Li, J. Luo and Z. Zhou, *Nat. Commun.*, 2022, **13**, 2193.
12 X. Wang, Y. W. Zhang, H. N. Si, Q. H. Zhang, J. Wu, L. Gao, X. F. Wei, Y. Sun, Q. L. Liao, Z. Zhang, K. Ammarah, L. Gu, Z. Kang and Y. Zhang, *J. Am. Chem. Soc.*, 2020, **142**, 4298–4308.
13 C. Tsai, H. Li, S. Park, J. Park, H. S. Han, J. K. Norskov, X. L. Zheng and F. Abild-Pedersen, *Nat. Commun.*, 2017, **8**, 15113.
14 Y. Li, Q. Gu, B. Johannessen, Z. Zheng, C. Li, Y. Luo, Z. Zhang, Q. Zhang, H. Fan, W. Luo, B. Liu, S. Dou and H. Liu, *Nano Energy*, 2021, **84**, 105898.
15 L. Jiang, Y. J. Zhang, X. H. Luo, L. Yu, H. X. Li and Y. J. Li, *Chem. Eng. J.*, 2021, **425**, 130611.
16 Y. Luo, L. Tang, U. Khan, Q. Yu, H. M. Cheng, X. Zou and B. Liu, *Nat. Commun.*, 2019, **10**, 269.
17 Y. T. Luo, X. Li, X. K. Cai, X. L. Zou, F. Y. Kang, H. M. Cheng and B. L. Liu, *ACS Nano*, 2018, **12**, 4565–4573.
18 S. Wang, D. Zhang, B. Li, C. Zhang, Z. G. Du, H. M. Yin, X. F. Bi and S. B. Yang, *Adv. Energy Mater.*, 2018, **8**, 1801345.
19 D. D. Zhu, J. L. Liu, Y. Q. Zhao, Y. Zheng and S. Z. Qiao, *Small*, 2019, **15**, 1805511.
20 P. Y. Kuang, T. Tong, K. Fan and J. G. Yu, *ACS Catal.*, 2017, **7**, 6179–6187.
21 Z. P. Lin, Z. P. Wang, S. J. Shen, Y. C. Chen, Z. X. Du, W. Y. Tao, A. J. Xu, X. F. Ye, W. W. Zhong and S. S. Feng, *J. Alloys Compd.*, 2020, **834**, 155217.
22 D. Z. Wang, X. Y. Zhang, S. Y. Bao, Z. T. Zhang, H. Fei and Z. Z. Wu, *J. Mater. Chem. A*, 2017, **5**, 2681–2688.
23 G. Q. Zhao, Y. Lin, K. Rui, Q. Zhou, Y. P. Chen, S. X. Dou and W. P. Sun, *Nanoscale*, 2018, **10**, 19074–19081.
24 M. H. Xing, S. K. Zhu, X. F. Zeng, S. T. Wang, Z. P. Liu and D. P. Cao, *Adv. Energy Mater.*, 2023, **13**, 2302376.
25 H. Xiong, C. F. Du, Z. L. Ma, R. C. Zhi, S. S. Hao, X. Y. Zhao, Z. Liu, F. Xu and H. Q. Wang, *Adv. Funct. Mater.*, 2024, **34**, 2402298.
26 Z. Chunhui, X. Zhe, H. Nana, T. Ye, K. Tanja, Y. Cunming and J. Lei, *Sci. Adv.*, 2023, **9**, eadd6978.
27 M. Hu, H. Chen, B. Liu, X. Xu, B. Cao, P. Jing, J. Zhang, R. Gao and J. Zhang, *Appl. Catal., B*, 2022, **317**, 121774.
28 W. Liu, X. T. Wang, F. Wang, K. F. Du, Z. F. Zhang, Y. Z. Guo, H. Y. Yin and D. H. Wang, *Nat. Commun.*, 2021, **12**, 6776.
29 J. Sun, S. Qin, Z. Zhang, C. Li, X. Xu, Z. Li and X. Meng, *Appl. Catal., B*, 2023, **338**, 123015.
30 L. Lai, J. Li, Y. Deng, Z. Yu, L. Wei and Y. Chen, *Small Struct.*, 2022, **3**, 2200112.
31 K. Murugappan, E. M. Anderson, D. Teschner, T. E. Jones, K. Skorupska and Y. Román-Leshkov, *Nat. Catal.*, 2018, **1**, 960–967.
32 J. A. Bau, R. Ahmad, L. Cavallo and M. Rueping, *ACS Energy Lett.*, 2022, **7**, 3695–3702.
33 C. Li, Z. Wang, M. Liu, E. Wang, B. Wang, L. Xu, K. Jiang, S. Fan, Y. Sun, J. Li and K. Liu, *Nat. Commun.*, 2022, **13**, 3338.